Japanese Journal of Applied Physics

BRIEF NOTE

Investigation on application of singular value decomposition filter in element domain for extraction of ultrasonic echoes from blood cells in jugular veins

Japanese Journal of Applied Physics **61**, SG1011 (2022) **BRIEF NOTE**
https://doi.org/10.35848/1347-4065/ac4680

Investigation on application of singular value decomposition filter in element domain for extraction of ultrasonic echoes from blood cells in jugular veins

Ryo Nagaoka[1*], Masaaki Omura[1], Michiya Mozumi[1], Kunimasa Yagi[2], and Hideyuki Hasegawa[1]

[1]*Faculty of Engineering, University of Toyama, Toyama 930-8555, Japan*
[2]*Faculty of Medicine, University of Toyama, Toyama 930-0194, Japan*

[*]E-mail: nryo@eng.u-toyama.ac.jp

Received November 2, 2021; revised December 7, 2021; accepted December 26, 2021; published online March 22, 2022

The singular value decomposition (SVD) based clutter filter is commonly applied to beamformed signals for the visualization of echo signals from flowing blood cells. In this paper, the SVD-based clutter filter is applied to signals directly acquired from ultrasonic elements before beamforming to be compared with the conventional strategy by evaluating contrast and standard deviation (SD) in the filtered images. As a result, the contrast was improved from 10.7 ± 3.6 dB to 18.3 ± 4.6 dB, and the SD was slightly improved from 3.78 ± 0.69 dB to 3.07 ± 0.74 dB in the measurement of a right jugular vein. © 2022 The Japan Society of Applied Physics

Singular value decomposition (SVD) based clutter filter[1–9] was developed for visualization of echo signals from blood flow in high temporal resolution ultrasonic measurements.[10–12] The SVD-based clutter filter commonly extracts desired components from beamformed signals based on both the spatial and temporal characteristics. In the procedure, the signals from the blood flow can be extracted by removing the undesired components, which corresponds to band pass filtering. By focusing on the temporal domain in this process, DC and noise components were suppressed using the clutter filter. Also, amplitudes of beamformed signals are important information in SVD clutter filtering. Meanwhile, in our previous study on measurement of a heart,[6] the SVD-based clutter filter was applied to the signals directly acquired from ultrasonic elements before beamforming, and the resultant filtered signals were compared with those obtained by applying the clutter filter to the beamformed signals (in this paper, the signals received at the channels are called as element signals). However, the image quality metrics, i.e. contrast-to-noise ratio (CNR), obtained by applying the clutter filter to the beamformed signals was superior to those obtained by applying the filter to the element signals. In this paper, the image quality metrics, i.e. contrast and standard deviation (SD) of the signals from flowing blood cells, were investigated when the SVD-based clutter filter was applied to the beamformed and element signals in the measurement of a jugular vein located in the shallower and narrower region than a heart. It would also be possible to estimate coherence factor[13] and average speed of sound[14–18] for blood flow images if the SVD-based clutter filter works well also for element signals. In our previous research,[19] only contrast was used for the comparison as an evaluation index. In this study, the contrast and SD were calculated for the comparison. Moreover, cutoff frequencies in the clutter filtering were also investigated in both the strategies.

The detailed procedure of the SVD-based clutter filter is described in the previous papers.[1–9] In this paper, the procedure is briefly explained. As described above, an objective of this paper is to compare the image quality metrics obtained by applying the filter to the beamformed signals (conventional strategy) with those obtained by applying the filter to the element signals (proposed strategy). In the conventional strategy, a spatiotemporal matrix $\mathbf{S}$ is created by rearranging the beamformed signals s_b of dimensions (N_x, N_z, N_n) to a 2-D matrix of dimensions ($N_x \times N_z$, N_n). Meanwhile, in the proposed strategy, a spatiotemporal matrix $\mathbf{S}$ is created by rearranging the element signals s_e of dimensions (N_i, N_t, N_n) to a 2-D matrix of dimensions ($N_i \times N_t$, N_n). Variables N_x, N_z, N_n and N_t are the number of sampling points in the lateral, depth directions, the packet size, and the number corresponding to an integer part of a value obtained by dividing the received time from the transmission of ultrasound by a sampling time, respectively. Also, variable N_i is the number of receiving element channels. Using SVD, the spatiotemporal matrix $\mathbf{S}$ can be decomposed into a product of three matrices as

$$\mathbf{S} = \mathbf{U}\mathbf{\Sigma}\mathbf{V}^{\mathrm{T}}. \tag{1}$$

The diagonal matrix $\mathbf{\Sigma}$ is composed of singular values in a descending order. Also, the matrices $\mathbf{U}$ and $\mathbf{V}$ are composed of spatial and temporal singular vectors, respectively. By replacing the singular value of the matrix $\mathbf{\Sigma}$ of the order lower or higher than thresholds with zero, the desired echo signals from red blood cells are extracted in the clutter filtering process. In this paper, the lower and higher thresholds were chosen based on the magnitude and slope of the profile of the singular value, respectively. The magnitude for the lower threshold was empirically set to −52 dB. The packet size N_n for the SVD-based clutter filter was set to 1024 frames. Also, the temporal window was shifted by a half of the packet size. In this study, mean frequencies (MFs) of the temporal singular vectors at the lower and higher thresholds were calculated using the following equation for the comparison as[7]

$$\mathrm{MF} = \frac{\sum_{i=1}^{N_n} f_i P_i}{\sum_{i=1}^{N_n} P_i}, \tag{2}$$

where a variable P_i is an amplitude of the power spectrum of the temporal singular vector at a frequency of f_i. The subscript i indicates the specific number of the power spectrum.

Echo signals were acquired using an ultrasonic programmable measurement system with 256 Tx-Rx channels (RSYS-0011, Microsonic Co., Ltd., Tokyo, Japan) and 7.5 MHz linear array ultrasonic probe (UST-5412, Fujifilm) consisting of 192 elements at a sampling frequency of 31.25 MHz. A high temporal ultrasonic imaging was achieved using plane wave imaging.[20] A Tukey window was used as an apodization function in plane wave transmission. To reconstruct B-mode images, Delay-And-Sum (DAS) beamforming was applied to the acquired element signals with a fixed F-number

of 1 in the conventional strategy. Also, to reconstruct blood flow images in the proposed strategy, the DAS beamforming was applied to the element signals after the clutter filtering with the same F-number of 1. The interval between transmissions was set to 96 μs, which corresponded to a frame rate of 10.4 kfps. The image quality was evaluated based on contrast of the blood flow image and SD of the signals from the blood flow for one cardiac cycle. The contrast of the blood flow image was defined as

$$\text{contrast} = \frac{\mu_{bf}}{\mu_t}, \tag{3}$$

where variables μ_{bf} and μ_t are mean amplitudes in regions of the blood flow and tissue including noise components, respectively. In this paper, right and left jugular veins of a 33-years-old healthy male were measured. This study was approved by the institutional ethical committee and performed with the informed consent of the subject.

Figure 1(a) shows a B-mode image of the right jugular vein. Also, Figs. 1(b) and 1(c) show the blood flow images of the right jugular vein obtained by the conventional and proposed strategies, respectively. In Fig. 1, red solid and blue dotted squares indicate the regions of interest (ROIs) in blood flow and tissues (including noise) for calculation of the contrast and SD. The positions of ROIs were determined manually. As shown in Fig. 1(c), speckle pattern was more clearly visualized and noise components were more suppressed using the proposed strategy. Figures 2(a) and 2(b) show the singular value profiles obtained by the conventional and proposed strategies, respectively. The profile obtained by the conventional strategy was different from that obtained by the proposed one. The MFs of the temporal singular vectors at the lower threshold obtained by the conventional and proposed strategies were 1319 ± 534 and 664 ± 86 Hz, respectively. Also, the MFs of the temporal singular vectors at the higher threshold obtained by the conventional and proposed strategies were 3176 ± 246 and 3300 ± 296 Hz, respectively. The higher thresholds were chosen adaptively based on the slope of the profile of the singular value by minimizing a mean squared difference α between the measured singular values σ_j and those $\hat{\sigma}_j$ obtained by fitting a linear function to the measured ones using the least squares method in a range from start index m_s to end index m_e .[21] Although the MFs of the components at the higher threshold were almost same independent of the strategies, the SD of the mean frequency obtained by the conventional strategy was larger than that obtained by the proposed strategy at the lower threshold. This trend was also observed in the measurement of the left jugular vein. As the blood flow in a vein can be considered a steady flow and surrounding tissues and vascular wall do not move so much, the mean frequency at the lower threshold corresponding to a boundary between tissue clutter and flow components is expected to be stable. As the measurement region includes common carotid artery, there is a possibility that movement of the arterial wall and blood flow in the artery influences the conventional clutter filtering. Figures 3(a) and 3(b) show contrast and SD of the signals from the blood flow obtained with both the strategies. As shown in Fig. 3, contrast of the blood flow image was improved, and the signals from the blood flow were more stably visualized using the proposed strategy. In the measurement of the right jugular vein, the contrast was improved from 10.7 ± 3.6 dB to 18.3 ± 4.6 dB, and the SD of the signals from the blood flow was slightly improved from 3.78 ± 0.69 dB to 3.07 ± 0.74 dB. Also, in the measurement of the left jugular vein, the contrast was improved from 6.41 ± 4.8 dB to 14.7 ± 5.2 dB, and the SD was slightly improved from 4.24 ± 0.96 dB to 3.86 ± 1.07 dB. These results indicated that the proposed strategy could improve the image quality metrics in the measurement of the jugular vein.

It was assumed that as a size of a red blood cell was much smaller than the wavelength of a transmission wave, signals spherically reflected from red blood cells, i.e. scattered components. Meanwhile, it is assumed that as a dimension of the walls is enough larger than the wavelength, the signals from the walls correspond to reflected components. Hence, this difference between the signals from red blood cells and wall might lead to the improvement of the image quality metrics using the proposed strategy. In other words, it is considered that the proposed strategy could extract the signals from red blood cells as scattered components while the conventional strategy could not separate the scattered and reflected components well. This difference might be caused by a larger order of approximately 210 for the lower threshold in the proposed strategy than

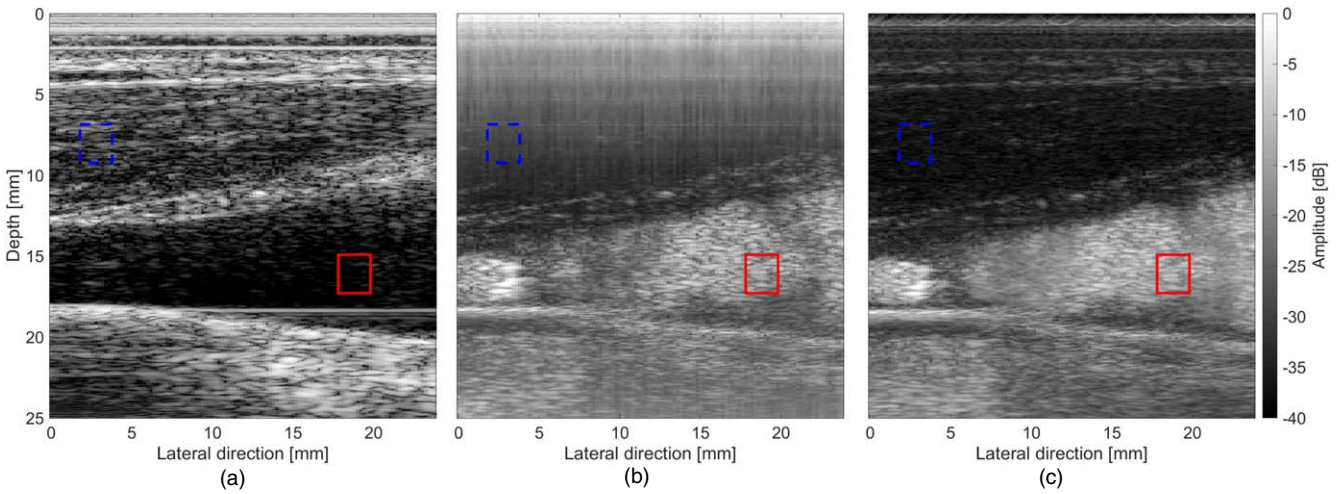

Fig. 1. (Color online) (a) B-mode image of the right jugular vein. Blood flow images of right jugular vein obtained by (b) the conventional and (c) proposed strategies. Red solid and blue dotted squares were ROIs of blood flow and tissues (including noise) for calculation of contrast and SD.

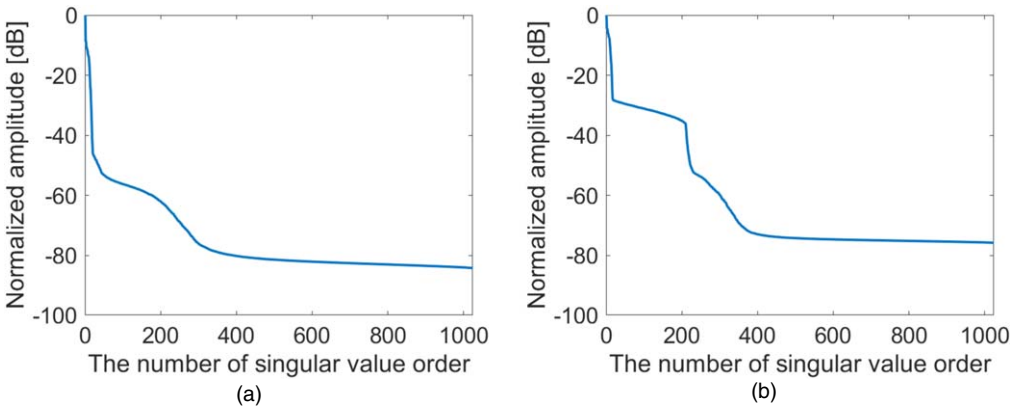

Fig. 2. (Color online) The singular value profiles obtained by (a) the conventional and (b) proposed strategies, respectively.

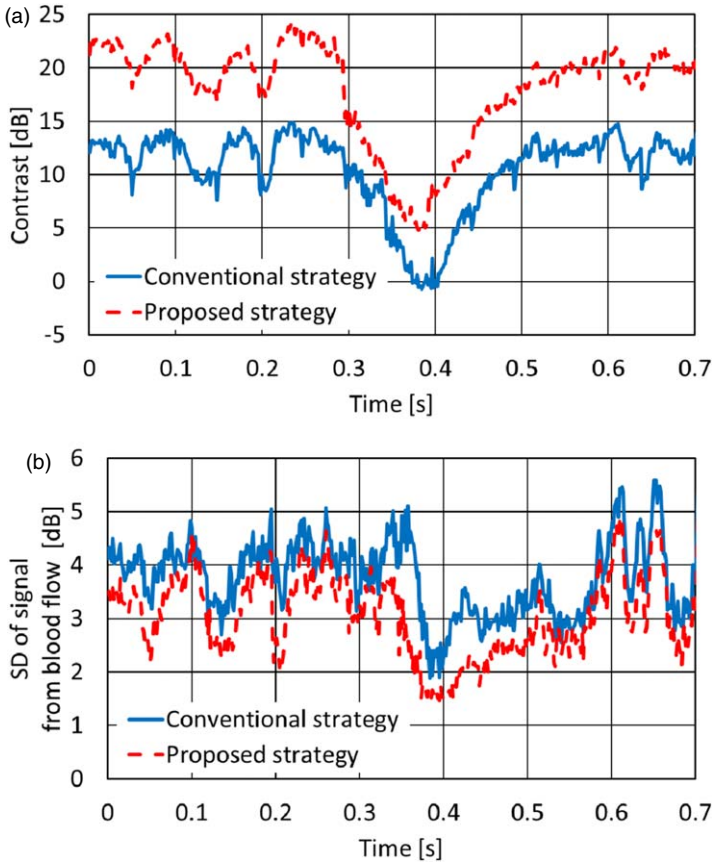

Fig. 3. (Color online) (a) Contrast and (b) SD of signal from blood flow obtained by both the strategies.

approximately 40 in the conventional one. Meanwhile, there is possibility that the ratio of the scattered component to the reflective component in the signals from red blood cells may change with the degree of aggregation. In our future work, this relationship will be investigated by performing simulations. In the simulations, the separability of both the strategies is compared based on the image quality metrics when the scatterer number density is changed.

In this study, the contrast and SD were calculated for the comparison. Also, the cutoff frequencies in the clutter filtering were investigated in both the strategies by evaluating the frequency components in the temporal singular vectors. In the measurement of both the right and left jugular veins, the contrast was improved and the SD of the signals from the blood flow was slightly reduced. Although the MFs of the temporal singular vectors at the higher thresholds were stable independent of the strategies, the mean frequency obtained by the conventional strategy was unstable. This trend was observed in the measurement of both the jugular veins. These results indicated that the proposed strategy was more preferable than the conventional strategy in measurement of veins.

Acknowledgments This study was supported by JSPS KAKENHI Grant No. 18KK0110, and JST Moonshot R&D Grant No. JPMJMS2021.

ORCID iDs Ryo Nagaoka https://orcid.org/0000-0002-6713-8106 Masaaki Omura https://orcid.org/0000-0002-4432-8548 Hideyuki Hasegawa https://orcid.org/0000-0003-0709-7821

1) C. Demené et al., IEEE Trans. Med. Imaging **34**, 2271 (2015).
2) P. Song, A. Manduca, J. D. Trzasko, and S. Chen, IEEE Trans. Med. Imaging **36**, 251 (2017).

3) P. Song, J. D. Trzasko, A. Manduca, B. Qiang, R. Kadirvel, D. F. Kallmes, and S. Chen, IEEE Trans. Ultrason. Ferroelectr. Freq. Control **64**, 706 (2017).
4) H. Ikeda, R. Nagaoka, M. Lafond, S. Yoshizawa, R. Iwasaki, M. Maeda, S. Umemura, and Y. Saijo, Jpn. J. Appl. Phys. **57**, 07LF12 (2018).
5) J. Baranger, B. Arnal, F. Perren, O. Baud, M. Tanter, and C. Demené, IEEE Trans. Med. Imaging **37**, 1574 (2018).
6) M. Mozumi, R. Nagaoka, and H. Hasegawa, Jpn. J. Appl. Phys. **58**, SGGE02 (2019).
7) H. Hasegawa, R. Nagaoka, M. Omura, M. Mozumi, and K. Saito, J. Med. Ultrason. **48**, 13 (2021).
8) M. W. Kim, Y. Zhu, J. Hedhli, L. W. Dobrucki, and M. F. Insana, IEEE Trans. Ultrason. Ferroelectr. Freq. Control **65**, 2020 (2018).
9) Y. Zhu, M. W. Kim, C. Hoering, and M. F. Insana, IEEE Trans. Ultrason. Ferroelectr. Freq. Control **67**, 1830 (2020).
10) M. Tanter, J. Bercoff, L. Sandrin, and M. Fink, IEEE Trans. Ultrason. Ferroelectr. Freq. Control **49**, 1363 (2002).
11) H. Hasegawa and H. Kanai, IEEE Trans. Ultrason. Ferroelectr. Freq. Control **55**, 2626 (2008).
12) G. Montaldo, M. Tanter, J. Bercoff, N. Benech, and M. Fink, IEEE Trans. Ultrason. Ferroelectr. Freq. Control **56**, 489 (2009).
13) P. C. Li and M. L. Li, IEEE Trans. Ultrason. Ferroelectr. Freq. Control **50**, 128 (2003).
14) M. Imbault, A. Faccinetto, B. F. Osmanski, A. Tissier, T. Deffieux, J. L. Gennisson, V. Vilgrain, and M. Tanter, Phys. Med. Biol. **62**, 3582 (2017).
15) H. Hasegawa and R. Nagaoka, J. Med. Ultrason. **46**, 297 (2019).
16) F. Sannou, R. Nagaoka, and H. Hasegawa, Jpn. J. Appl. Phys. **59**, SKKE14 (2020).
17) W. Lambert, L. A. Cobus, M. Couade, M. Fink, and A. Aubry, Phys. Rev. X **10**, 021048 (2020).
18) R. Nagaoka, S. Yoshizawa, S. Umemura, and H. Hasegawa, Jpn. J. Appl. Phys. **60**, SDDE19 (2021).
19) R. Nagaoka, M. Omura, M. Mozumi, K. Yagi, and H. Hasegawa, Proc. U.S. E. **42**, 1Pa5-4 (2021).
20) R. Nagaoka, K. Ishikawa, M. Mozumi, M. Cinthio, and H. Hasegawa, Jpn. J. Appl. Phys. **59**, SKKE16 (2020).
21) R. Nagaoka and H. Hasegawa, J. Med. Ultrason. **46**, 187 (2019).